In Situ Monitoring of Nanoparticle Formation: Antisolvent Precipitation of Azole Anti-fungal Drugs

Kate P. M. McComiskey[1], Naila A. Mugheirbi[2], Jack Stapleton[2], Lidia Tajber[1]*

[1] Synthesis and Solid State Pharmaceutical Centre, School of Pharmacy and Pharmaceutical Sciences, Trinity College Dublin, Dublin 2, Ireland.

[2] School of Pharmacy and Pharmaceutical Sciences, Trinity College Dublin, Dublin 2, Ireland.

*School of Pharmacy and Pharmaceutical Sciences, Trinity College Dublin, College Green, Dublin 2, Ireland. Tel: +35318962787. Fax: +35318962810. Email: ltajber@tcd.ie

Abstract

In this work we report the effect of stabilizer choice and concentration on nanoparticle (NP) stability over time. Three different BCS class II active pharmaceutical ingredient (APIs): itraconazole (ITR), ketoconazole (KETO) and posaconazole (POS) were chosen due to their poor aqueous solubility and closely related chemical structures. Polyethylene glycol, polyethylene glycol methyl ether and polyethylene glycol dimethyl ether (DMPEG) with a molecular weight of 2,000 Dalton were included as stabilisers. NPs were formed *in situ* using an anti-solvent addition, bottom up method at 25 °C. Colloidal stability was monitored using dynamic light scattering (DLS), accompanied by morphological examination of the NPs using scanning electron microscopy. Kinetic modelling indicates nanoparticle growth is driven by Ostwald ripening (OR). The presence of DMPEG causes OR growth to become an interface controlled process following a parabola trend. DMPEG encourages OR for POS NPs whilst driving the crystallisation process. The rate of OR appears to be inherent of the crystallisation pathway by which these APIs proceed. Crystallization mechanisms are API, stabilizer type and concentration dependent. DLS is suitable as an initial systematic screening method for stabilizer selection, aiding the pharmaceutical scientist in the optimisation of nano-formulations.

Keywords: itraconazole, posaconazole, ketoconazole, Ostwald ripening, dynamic light scattering, nanoparticle, crystallization

Chemical compounds studied in this article:

Itraconazole (PubChem CID: 55283); Ketoconazole (PubChem CID: 47576); Posaconazole (PubChem CID: 468595); Poly(ethylene glycol) (PubChem CID: 24887695); Poly(ethylene glycol) methyl ether (PubChem CID: 24852095); Poly(ethylene glycol) dimethyl ether (PubChem CID: 24868206)

List of abbreviations

API = active pharmaceutical ingredient

BCS = biopharmaceutical classification system

Da = Dalton

DCS = developability classification system

DLS = dynamic light scattering

DMPEG = polyethylene glycol dimethyl ether

HPLC = high performance liquid chromatography

ITR = itraconazole

KETO = ketoconazole

LLPS = liquid-liquid phase separation

MPEG = polyethylene glycol methyl ether

NP = nanoparticle

OA = orientated attachment

OR = Ostwald ripening

PDI = polydispersity index

PEG = polyethylene glycol

POS = posaconazole

PSD = particle size distribution

PXRD = powder x-ray diffraction

RSD = relative standard deviation

S = supersaturation ratio

SD = standard deviation

SEM = scanning electron microscopy

1. Introduction

It has been reported in literature that 40% of marketed drugs suffer from poor aqueous solubility thereby limiting their dissolution in biological fluids. As a result, we have new chemical entities with poor bioavailability and erratic absorption (Shegokar and Müller, 2010). Nanosization i.e. production of nanoparticles, has emerged as a promising strategy for optimizing bioavailability of hydrophobic drugs.

Reduction of particle size results in an increase in surface area available for dissolution (Noyes and Whitney, 1897). Small particles with a high surface curvature exhibit high saturation solubility (Ostwald, 1900). This gives rise to Ostwald ripening phenomenon, whereby particles which possess a degree of solubility in the dispersed phase are thermodynamically unstable. The system will move to reduce the interfacial energy via particle growth. Consequently, larger particles grow as the result of the re-dissolution of smaller more soluble particles (Voorhees, 1985). For this reason, physical stability of resultant nanoparticles remains a challenging aspect of successful nano-dispersion product development. NP production methods can be categorised as top down or bottom up. Wet milling is a common top down method avoiding organic solvent use and benefitting from easy scale-up (Van Eerdenbrugh et al., 2008). However common problems associated with this technique include degradation and stability. In contrast, bottom up approaches such as anti-solvent precipitation allow for fine tuning of product characteristics such as morphology and crystallinity, with simplicity and cost also being noted as advantages (Zhang et al., 2009).

Other processes affecting the physical stability of nano-dispersions include flocculation, a reversible process whereby particles aggregate but remain as individual particles and coalescence is the process by which two or more particles merge during contact resulting in the formation of a single particle. Once in contact a pair or group of NPs will coalesce to reduce their surface energy. Surface processes control coalescence. Coalescence is an irreversible process (Ingham et al., 2011). In addition, the high surface area of drug nano-dispersions promotes nucleation and crystal growth resulting in instability

(Dolenc and Kristl, 2009). Crystal growth can occur during the production and shelf life of nano-dispersions which can adversely affect their dissolution behaviour and *in vivo* performance (Ghosh et al., 2012). Inclusion of a suitable stabilizer can maintain colloidal stability, therefore avoiding aggregation and Ostwald ripening (OR). However, stabilizer selection has remained a challenge due to the lack of fundamental understanding surrounding interactions within colloidal systems. For this reason, systematic stabilizer selection offers pharmaceutical companies attractive gains in terms of time and cost. Stabilizers act to inhibit aggregation within nano-dispersions via two methods, electrostatic repulsion or steric stabilization. Polymers work via steric stabilization, whereby, adsorption of stabilizer molecules onto particle surfaces creates physical barriers which hinder van der Walls attractive forces between neighbouring particles (Palla and Shah, 2002). Polymeric stabilizers can have numerous sites in their chains with affinity for active pharmaceutical ingredient (API) surfaces therefore polymer chain morphology determines conformation of adsorption. With stabilizers adsorbed onto the particle surface through the anchor segment, good solvation between the solvent and the stabilizing segment of the stabilizer is required to achieve steric stabilization and prevent particles from agglomerating in the dispersion medium. Stabilizer adsorption can occur in a number of ways: van der Waals forces, ion-dipole interaction, ionic interaction, hydrogen bonding, or by hydrophobic effect (Mahesh et al., 2014). Current literature highlights the benefits offered by polyethylene glycol (PEG) as a stabilizer. Not only is PEG low in cost, it also possesses a good in vivo safety profile (Mugheirbi et al., 2014).

For efficient nanoparticle (NP) application it is necessary to fully understand the crystallization pathways and growth kinetics responsible for the evolution of those NPs. NP coarsening was first described using the OR mechanism mentioned above, whereby crystal growth is controlled by diffusion (Wagner, 1961; Speight, 1968; Kirchner, 1971). The unique kinetics of crystallization pathways involving NPs have led to the exploration of alternative crystal growth models, namely orientated attachment (OA) based crystal growth. OA growth occurs when two crystallographically oriented NPs combine to the form a larger single crystal. Resulting particles are generally irregular in

shape, in contrast to those arising from OR which tend to be spherical in shape (Huang et al., 2003a). In addition, OA tends to follow an asymptotic curve whilst OR growth generally follows a parabola trend (Wagner, 1961; Speight, 1968; Kirchner, 1971). Two-stage crystal growth has been observed whereby asymptotic growth described by the OA growth model, was followed by cubic parabola growth well described by the OR growth model (Huang et al., 2003a). Elsewhere in the literature, the phenomena of hybrid crystal growth has been described by a model accounting for both OA and OR physical processes occurring simultaneously in a competitive manner (Huang et al., 2003a; Yin et al., 2011). For this reason, it can be difficult to study the growth kinetics of such NPs. The role of surface adsorption in such processes has been explored, with strong surface adsorption being found to promote OA whilst delaying OR growth (Yin et al., 2011). It has been proposed that OA occurs via three steps; diffusion of NPs in solution followed by collision, then desorption of surface ligands and finally coalescence. Therefore factors such as surface properties of the NPs and particle-particle interactions can play a part in these events (Huang et al., 2003b).

Itraconazole (ITR), posaconazole (POS) and ketoconazole (KETO) are azole anti-fungal compounds which can be categorised as Biopharmaceutical Classification System (BCS) class II drugs. Butler et al., have recently proposed a revised classification system, the developability classification system (DCS). This system divides BCS Class II compounds into IIa and IIb, where IIa compounds are said to be dissolution rate limited, whereby drug particles cannot dissolve in the time it takes to pass their absorption site. On the other hand, IIb compounds are solubility limited, whereby there is an inadequate volume of fluid available in the gastrointestinal tract to dissolve the administered dose (Butler et al. 2010). ITR has an aqueous solubility below 1 µg/ml (Matteucci et al., 2009) while, POS and KETO are both poorly soluble in water (Dressman and Reppas, 2000). For this reason, it is likely that ITR is solubility limited, responsible for its limited dissolution while POS and KETO are dissolution rate limited. For this reason, these APIs are ideal candidates for particle size reduction techniques.

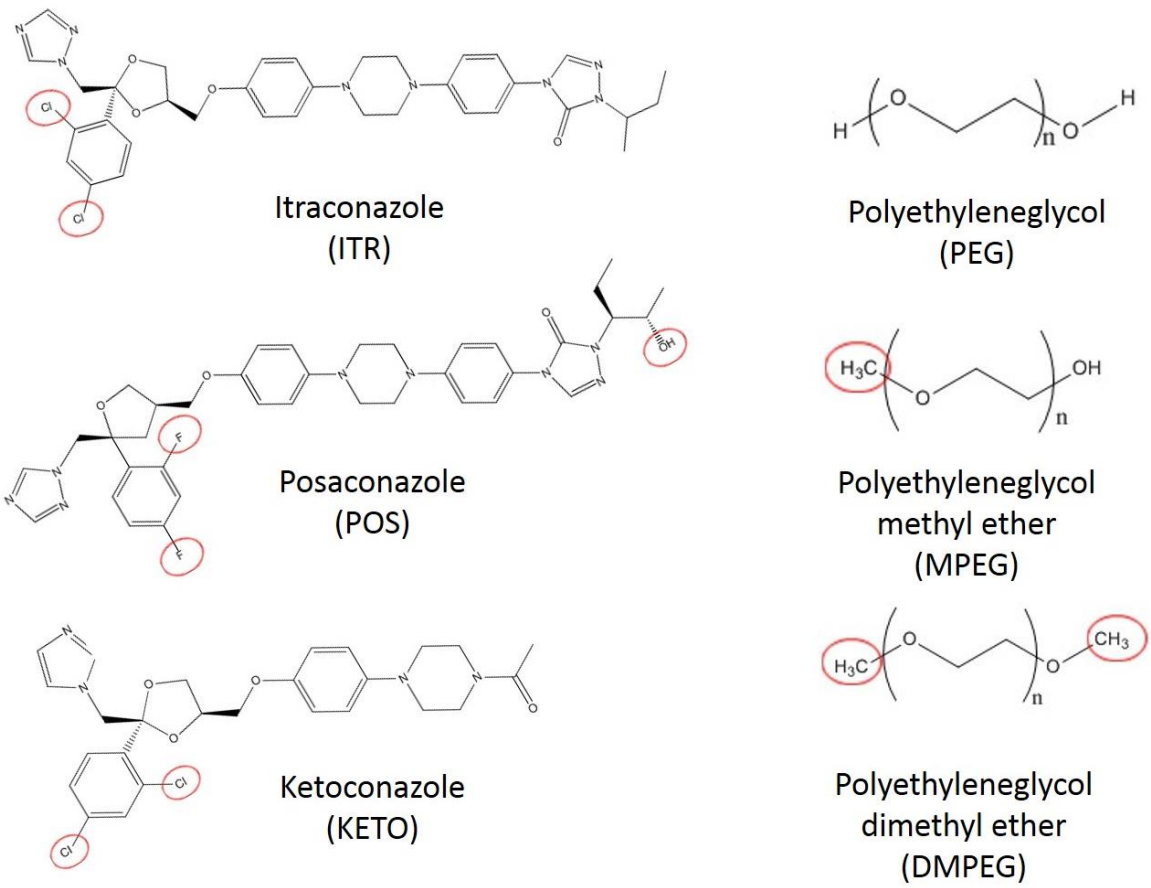

Fig. 1. Chemical structure of APIs and stabilizers. Red circles highlight important parts of structures.

Currently, the selection of optimum stabilizer for nanodispersions is achieved via a trial and error approach. A systematic screening method for stabilizer selection should be simple to execute in a quick manner, whilst providing a wealth of information regarding the NPs under analysis. Dynamic light scattering (DLS) was successfully employed as a means of aiding stabilizer selection for antifungal azole BCS class II drugs; ITR, KETO and POS (Fig. 1). Polyethylene glycol (PEG), polyethylene glycol methyl ether (MPEG) and polyethylene glycol dimethyl ether (DMPEG) with a molecular weight of 2,000 Dalton (Da) were investigated as stabilisers (Fig. 1). We report the effect of stabilizer choice and its concentration on particle size, indicative of colloidal stability. In addition, derived mean count rate was noted. This is a measure of scattered light intensity which is proportional to particle concentration (Shang and Gao, 2014). Morphological examination of NPs was performed via scanning electron microscopy (SEM), and solid state transformations were monitored via powder X-ray diffraction

(PXRD). Kinetic modelling was utilised as a tool for strengthening our understanding surrounding the effect of stabilizer choice and concentration on the OR process (Ostwald, 1900; Voorhees, 1985).

2. Materials and methods

2.1 Materials

Itraconazole (ITR) was a gift from Welding GmbH (Hamburg, Germany). Ketoconazole (KETO) and posaconazole (POS) were purchased from Glentham Life Sciences Ltd. (Wiltshire, UK). Potassium dihydrogen phosphate reagent, poly(ethlyene glycol) (PEG), poly(ethylene glycol) methyl ether (MPEG) and its dimethoxylated derivative (DMPEG) with average molecular weights of 2,000 Da were purchased from Aldrich Chemical Co., Ltd. (Dorset, UK). Methanol HPLC grade was purchased from Fisher Scientific (Loughborough, UK). Acetone and acetonitrile Chromasolv® HPLC grade was obtained from Sigma Aldrich (Dorset, UK). MilliQ water was used in all instances. Potassium hydroxide pellets were purchased from Merck KGaA (Darmstadt, Germany).

2.2 Methods

2.2.2 Anti-Solvent Formation of ITR, POS and KETO Nanoparticles

Solutions of drugs dissolved in acetone (solvent phase) and water or a polymer/stabilizer solution (anti-solvent phase) were maintained at 25 °C and filtered using 0.45 µm syringe polytetrafluoroethylene (PTFE) filter (VWR, Ireland) prior to NP formation. Stabilizers were included at the following concentrations: 0.5 (0.05 % w/v), 1 (0.1 % w/v) and 1.5 mg/ml (0.15 % w/v).

NPs were formed in a 12 o.d. mm square glass cuvette (part number PCS8501) with anti-solvent added first, followed by rapid addition of a solvent phase forming NP dispersions at 25 °C. Solvent phase consisted of 70-80% saturated solution of API in acetone. The exact conditions of NP formation were dependent on the drug used. ITR NPs were formed using a solvent phase (2.0 mg/ml ITR in acetone = 80% saturated solution) into an anti-solvent phase, using a 1:10 solvent to anti-solvent (v/v) ratio (0.1 ml solvent phase added to 0.9 ml anti-solvent phase). POS NPs were formed by rapid mixing of a

solvent phase (14.8 mg/ml POS in acetone = 75% saturated solution) into an anti-solvent phase, using a 1:12.5 solvent to anti-solvent (v/v) ratio (0.08 ml solvent phase added to 0.92 ml anti-solvent phase). KETO NPs were formed by rapid mixing of a solvent phase (3.75 mg/ml KETO in acetone = 70% saturated solution) into an anti-solvent phase, using a 1:10 solvent to anti-solvent (v/v) ratio (0.1 ml solvent phase added to 0.9 ml anti-solvent phase).

2.2.3 Dynamic Light Scattering (DLS)

The mean particle size and polydispersity indices of NPs formed as per Section 2.2.2 were measured using the Zetasizer Nano ZS series (Malvern Instruments, UK) as described by (Mugheirbi et al., 2014) without further dilutions. Measurement position and attenuator factor were automatically optimised by the software. All measurements were carried out at 25 °C in a 1 ml glass cuvette (part number PCS8501). The analysis was performed in triplicate for each sample. Viscosity of the continuous phase was measured using a Vibro Viscometer SV-10 (A&D, Japan) and the size values corrected for the actual viscosity of the dispersion medium.

2.2.4 Determination of solubility of APIs in acetone and deionised water

Solubility of APIs in acetone and deionised water was obtained as follows. Excess API was added to the solvent of interest in a closed glass vial and allowed to equilibrate overnight with continuous stirring at 1000 rpm with temperature maintained at 25 °C. Samples in acetone were filtered through a 0.45 µm PTFE syringe filter (VWR, Ireland). Whereas, samples in water were centrifuged for 1 hour at 25 °C, 13000 rpm using a Thermo Scientific Heraeus Fresco 17 centrifuge. All samples were diluted appropriately and concentrations determined via HPLC (as described in Section 2.2.5). It should be noted that ITR solubility in water at 25 °C was obtained from literature (Matteucci et al., 2009). The solubility values are presented in Table 1.

2.2.5 High Performance Liquid Chromatography (HPLC)

The concentrations of ITR, POS and KETO in acetone and deionised water were measured using a Waters Symmetry® C_{18} 5 µm (4.6 mm x 150 mm) column attached to a Waters HPLC system equipped

with a Waters 2695 separations module and a 2996 photodiode array detector (ITR λ = 260 nm, POS λ = 260 nm, KETO = 240 nm).

For ITR mobile phase used consisted of acetonitrile: buffer pH 6.8 (60:40) (v/v). A 0.1M phosphate buffer solution was prepared by dissolving 6.8 mg of potassium dihydrogen phosphate in 1L of deionised water. 1M potassium hydroxide solution was prepared by dissolving 5.6 g of potassium hydroxide in 0.1L of deionised water, this solution was used to adjust the phosphate buffer pH to 6.8. For POS and KETO, mobile phase used consisted of methanol: water (75:25) (v/v). A flow rate of 1 ml/min and run time of 14 minutes was used in all cases. For the solubility of all APIs in deionised water a 100 µl injection volume was due to low solubility. For solubility studies of ITR in acetone, a 50 µl injection volume was used. For solubility studies of POS and KETO in acetone, a 20 µl injection volume was used. For the aqueous solubility determination calibration curves used were in the concentration range of 0.05 to 1 mg/ml. For solubility in acetone determination calibration curves were used in the range 2 to 20 mg/ml. Column temperature was maintained at 25 °C for the duration of separation using a column heater.

2.2.6 Scanning electron microscopy (SEM)

A Zeiss Ultra variable pressure field emission scanning electron microscope (Germany) equipped with a secondary electron detector and accelerating voltage of 5 kV was used for morphological examination of ITR nanoparticles. NP formulations were centrifuged at 4 °C for 10 min at 12,000 rpm using an Eppendorf 5810R centrifuge (Hamburg, Germany). The supernatant was removed and the remaining material was washed using deionised water. Aliquots of nano-dispersions were directly placed on aluminium stubs dried using nitrogen purge. Prior to examination sample were sputter coated with gold palladium under vacuum prior to analysis.

2.2.7 Powder X-ray diffraction (PXRD)

NPs were formed, centrifuged at 4 °C for 1 minute at 13,000 rpm using a Thermo Scientific Heraeus Fresco 17 centrifuge. The supernatant was discarded and pellet examined using a Rigaku Miniflex II,

desktop X-ray diffractometer (Japan) equipped with a Cu Kαradiation X-ray source. The samples were mounted on a low background silicon sample holder and scanned over a 2θ range 2-40°.

3 Results

3.1 Particle formation and size evolution

3.1.1 Stabilizer-free NPs

Table 1 demonstrates that POS possesses the greatest solubility in both acetone and water, in contrast with ITR having the lowest. In addition, it should be noted that POS aqueous solubility is 2-fold greater than that of KETO and 200-fold greater than that of ITR.

Table 1. Solubility of APIs in acetone and water along with theoretical supersaturation ratio (S) at 25 °C.

API	Solubility in acetone (mg/ml)	Solubility in water (mg/ml)	Supersaturation ratio (S) (API solubility in acetone/API Solubility in water)
ITR	2.5 ± 0.4	0.001*	2500
POS	19.7 ± 2.3	0.2 ± 0.006	98.5
KETO	5.2 ± 0.03	0.1 ± 0.03	52

* value taken from Matteucci et al., (2009)

Table 2 shows that upon initial NP formation stabilizer free ITR NPs are the smallest in size (155 ± 14 nm) with great reproducibility indicated by low standard deviation (SD) and relative standard deviation (RSD) of 14 and 9%, respectively. In contrast, POS NPs are the largest in size (308 ± 66 nm), with large variability in size (RSD of 21%). Therefore, even very small changes within the API structure can lead to NPs with entirely different sizes.

Table 2. Initial mean particle size (nm) for ITR, POS and KETO NPs measured immediately after particle formation, with 0.5 mg/ml stabilizer and without stabilizer included.

	ITR mean particle size ± SD (nm)	ITR PDI ± SD	POS mean particle size ± SD (nm)	POS PDI ± SD	KETO mean particle size ± SD (nm)	KETO PDI ± SD
Stabilizer free	155 ± 14	0.07 ± 0.05	308 ± 66	0.03 ± 0.03	200 ± 34	0.06 ± 0.03
PEG 0.5 mg/ml	197 ± 74	0.09 ± 0.04	262 ± 23	0.06 ± 0.03	507 ± 130	0.10 ± 0.01
MPEG 0.5 mg/ml	152 ± 13	0.08 ± 0.04	318 ± 28	0.07 ± 0.03	310 ± 85	0.12 ± 0.05
DMPEG 0.5 mg/ml	237 ± 32	0.10 ± 0.04	243 ± 13	0.07 ± 0.04	221 ± 17	0.07 ± 0.05

SD: standard deviation, PDI: polydispersity index

Fig. 2 presents an intensity based particle size distribution (PSD) obtained using DLS for stabilizer free ITR NPs. Three distinct NP size populations exist over the 30 minutes (labelled a, b and c), of subsequent increasing particle size. In addition, slight peak broadening between 0 and 30 minutes would suggest increasing polydispersity between these particle populations, consistent with data presented in Table 2.

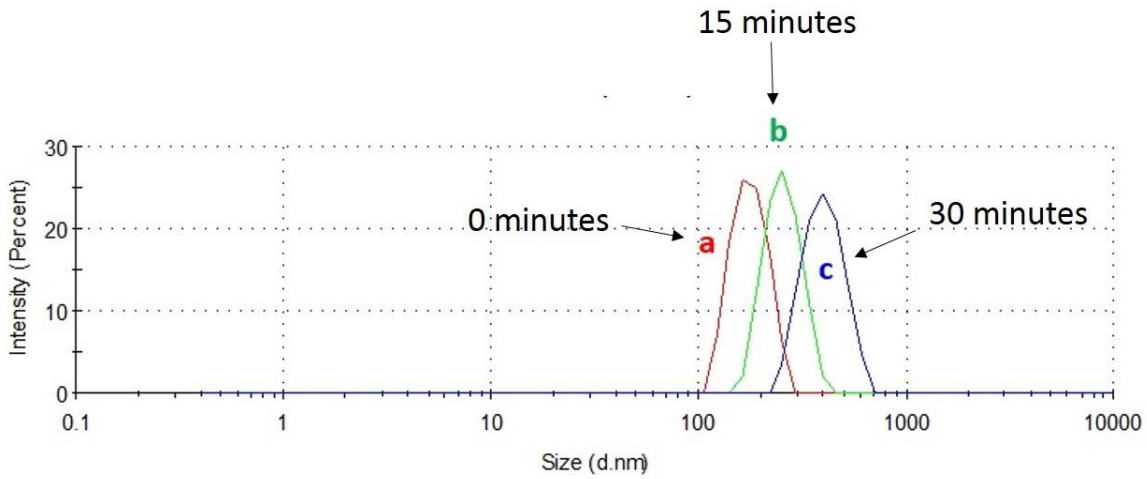

Fig. 2. DLS intensity based particle size distribution at (a) 0 (b) 15 and (c) 30 minutes for ITR stabilizer free NPs.

Fig. 3 shows that stabilizer free ITR NPs have the greatest colloidal stability over time, while stabilizer free KETO NPs are the least stable, as indicated by the large error bars for the size values present beyond 15 minutes. While ITR NPs doubled their size by 30 minutes of the experiment and POS NPs grew by 200%, KETO particles displayed very erratic and non-reproducible behaviour in terms of size. When we consider the supersaturation values for the APIs (Table 1), KETO and POS have relatively low S values (52 and 98.5, respectively), when compared with ITR (Table 1). ITR NP formation can be related to its limited miscibility in water, as its hydrophobic molecules are unable to form energetically favourable interactions with water, leading to aggregation of the molecules and the formation of a drug-rich phase i.e. ITR NPs dispersed within a continuous liquid phase (Ilevbare and Taylor, 2013). Nanocrystal growth in solution follows three steps: supersaturation and nucleation followed by crystal growth. Growth from solution results from a supersaturated medium generating a high rate of

nucleation leading to the burst of nuclei formation in a short period, an initial fast rate of growth of these nuclei and an eventual slow rate of growth leading to a long growth period (Viswanatha and Sarma, 2007). It appears that a high S ratio might be necessary for the formation of stable NPs made of APIs studied.

Sample scattering intensity is represented by count rates, here shown as derived count rates accounting for different signal attenuation levels, which are dependent upon both particle size and particle concentration (Shang and Gao, 2014). Fig. 3c shows a decreasing count rate trend for all stabilizer free NPs, this is indicative of particle instability, most likely sedimentation and/or aggregation. Such instability of NPs may be addressed via the addition of a stabilizer to the system (Van Eerdenbrugh et al., 2009).

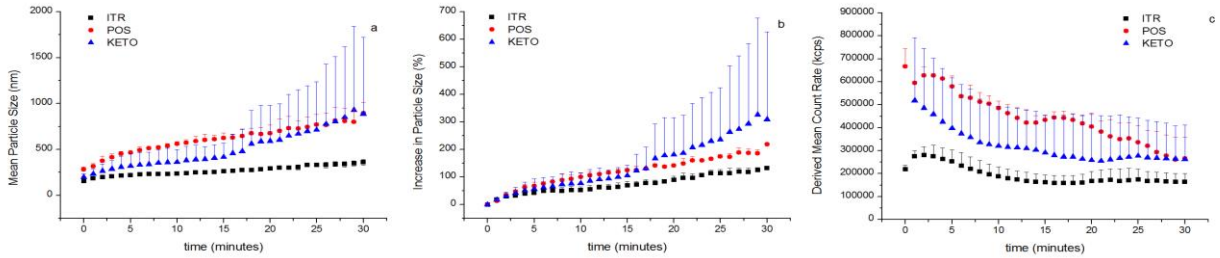

Fig. 3. Plots showing (a) mean particle size (nm) (b) increase in particle size (%) (c) derived mean count rate (kcps), for stabilizer free NPs.

3.1.2 Polymer-stabilised NPs

Initial experiments with polymers as NP stabilizers were carried out using 0.5 mg/ml of PEG, MPEG and DMPEG, results of which indicated variable success in achieving stable formulations. ITR NPs remained the smallest in size when stabilized with PEG and MPEG 0.5 mg/ml concentration (< 200 nm, Table 2). Interestingly, when DMPEG at 0.5 mg/ml is used as a stabilizer, KETO NPs are the smallest in size upon initial formation compared with ITR and POS NPs. All nanodispersions in this case can be described as having low polydispersity (Rane et al. 2005). Examples of particle size distributions for

nanodispersions stabilized by polymers can be found within Fig. SI. 1-3. Based on these initial results, a wider range of polymer concentration was explored. It is evident from the literature that common stabilizer concentrations range between 0.0125 % and 5 % w/v (Mugheirbi et al., 2014).

While ITR NPs presented relativity good stability even when no stabilizer was used, tests with polymers were conducted to explore if superior colloidal stability can be achieved. Fig. 4 presents a stabilizer type and concentration comparison for ITR NPs, including mean particle size (nm) and increase in particle size (%) data. Fig. 4b demonstrates PEG to be an effective stabilizer for ITR NPs when used at 1 mg/ml, as demonstrated by the low increase in particle size over 30 minutes. In Fig. 4d we can see that all ITR NPs stabilized with MPEG exhibit more than a 50% increase in particle size. Fig. 4e and f highlights DMPEG to be an ineffective stabilizer for ITR NPs when used at 1.5 mg/ml, however NP stabilization is favourable when concentrations below this are employed (Fig. SI. 4). In general, biphasic NP growth was observed consistently across all concentrations, with an initial rapid increase in particle size followed by a slower particle growth phase (Fig. 4b, d, f). In general, an initial burst/increase in count rate was seen upon ITR NP formation at 0 minutes, followed by a decline and eventual plateau in count rate (Fig. SI. 5). These events are likely to accompany rapid nucleation followed by a slower particle growth phase.

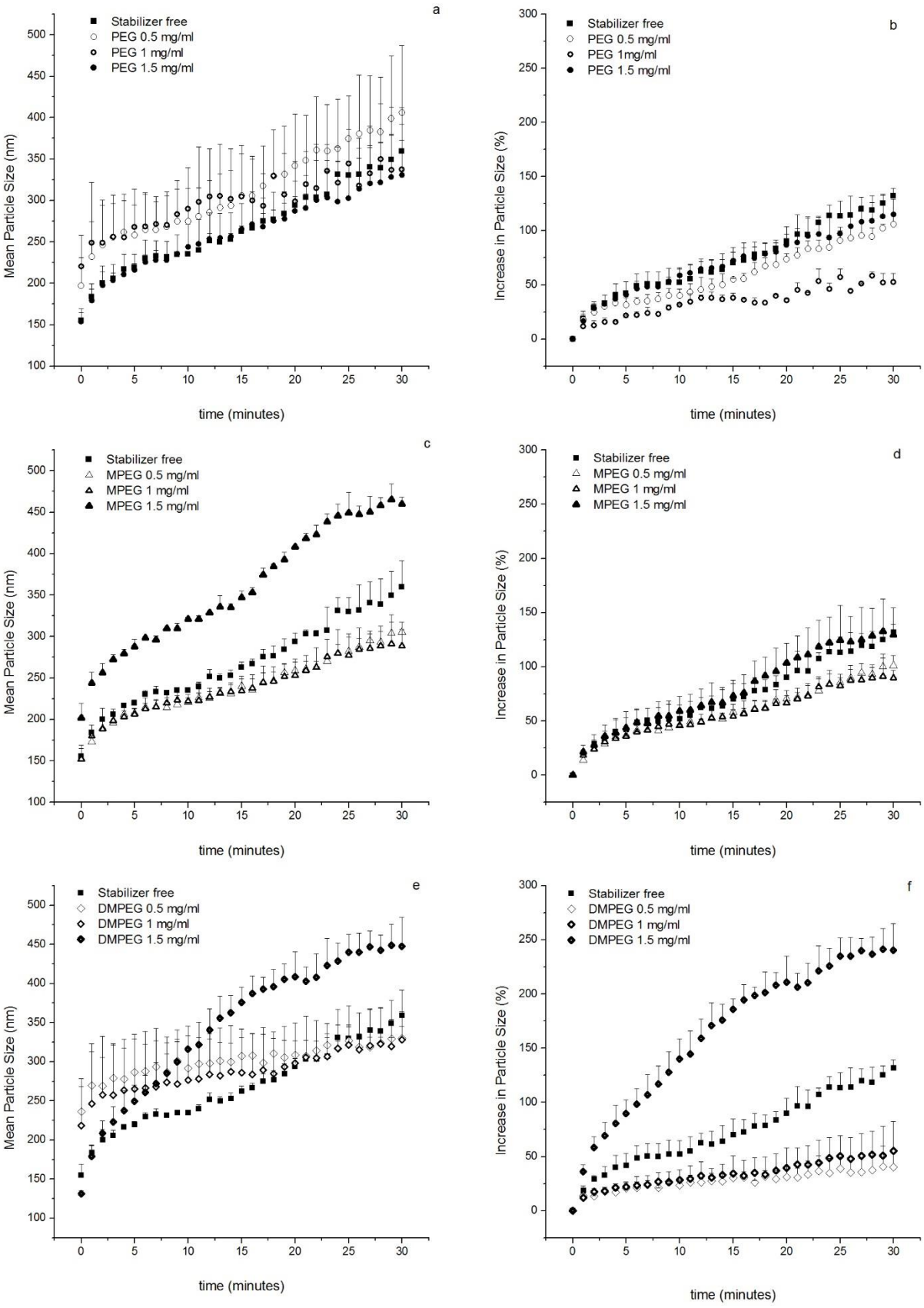

297

298 **Fig. 4.** Mean particle size (nm) and increase in particle size (%) versus time (minutes) for ITR NPs
299 stabilized with (a and b) PEG (c and d) MPEG and (e and f) DMPEG.

Fig. 5 presents mean particle size (nm) and increase particle size (%) data for POS NPs. The most stable systems were observed when DMPEG was included as a stabilizer or in the absence of a stabilizer (Fig. 5e and f). This was confirmed by a smaller increase in particle size (%) observed in these circumstances. POS NPs initially form around 200 nm (Fig. 5e). After 30 minutes NPs were generally above 1 micron in size as Fig. 5 shows. Extremely large particle sizes were observed after 30 minutes when PEG and MPEG were utilised as stabilizers (Fig. 5a and c) with POS NPs visibly precipitating at ~ 15 minutes. DMPEG was the most effective stabilizer for POS NPs, with particle size remaining ~ 1 micron at 30 minutes (Fig. 5e and f). Count rate trends for POS NPs also reflect the great variability as shown in Fig. SI. 6.

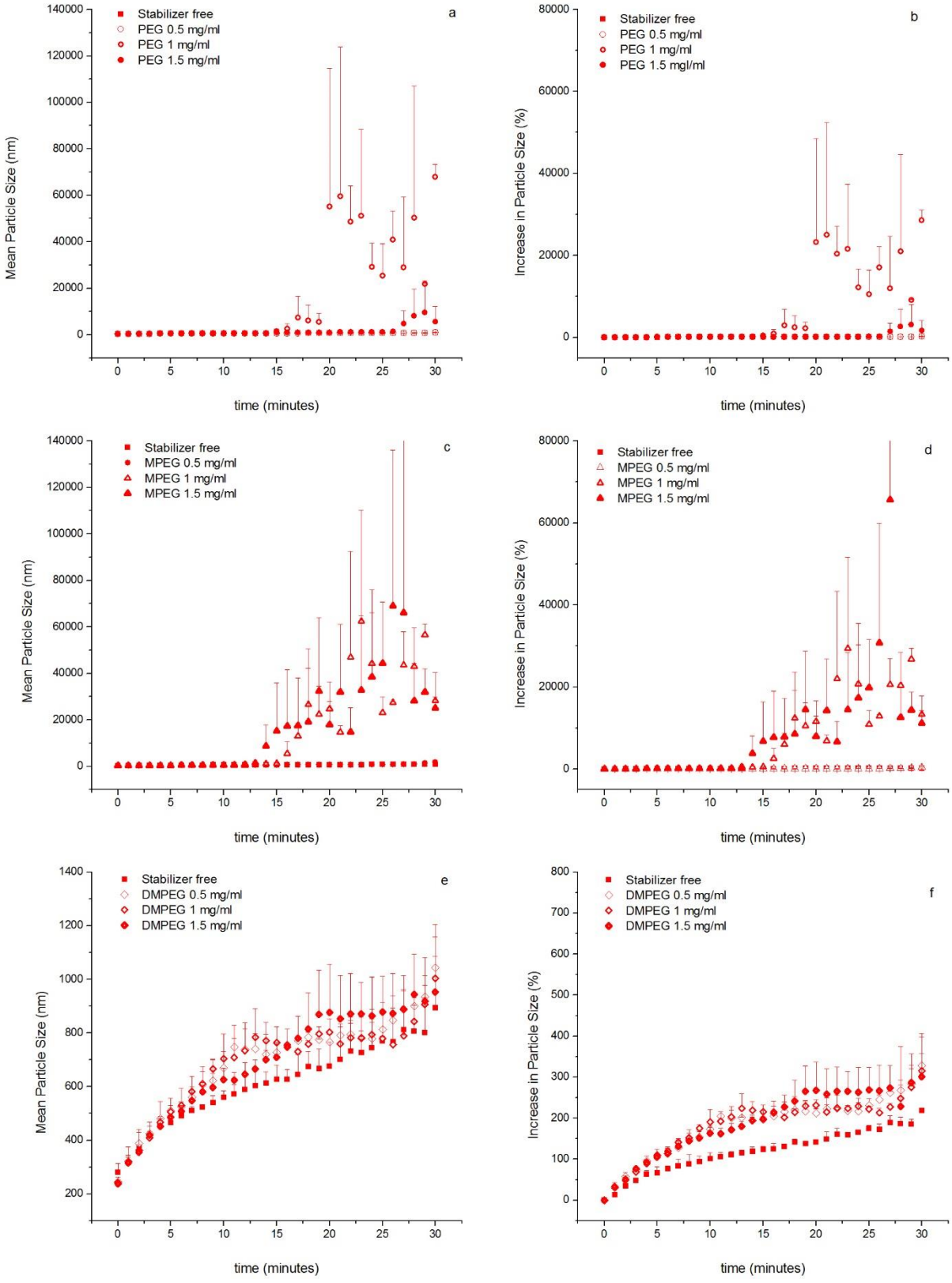

Fig. 5. Mean particle size (nm) and increase in particle size (%) versus time (minutes) for POS NPs stabilized with (a and b) PEG (c and d) MPEG and (e and f) DMPEG.

Fig. 6 presents mean particle size (nm) and increase particle size (%) data for KETO NPs. When PEG and MPEG were used as stabilizers, upon initial formation KETO NPs form ~ 250 -500 nm. At 30 minutes NPs are > 1500 nm (Fig. 6a and c). In contrast, when DMPEG was used as a stabilizer initial NPs form ~ 207 – 221 nm as shown by Fig. 7e. At 30 minutes DMPEG stabilized NPs < 1 micron (Fig. 6e). We can conclude from mean particle size data that DMPEG is the most effective stabilizer at maintaining colloidal stability of KETO NPs, with 1.5 mg/ml being the most effective concentration (Figure 6c). Fig. SI. 7 reiterates the general trend of falling count rates observed across all KETO NPs systems. Colloidal stability is shown to be concentration dependent when PEG is used as a stabilizer for KETO NPs. This is confirmed by increasing particle size (%) observed when PEG concentration is increased (Fig. 6b). Again, biphasic NP growth was seen across all KETO systems with an initial burst in size followed by a slower growth phase (Fig. 6b, d and f). As shown by Fig. 6f, DMPEG is the most effective stabilizer for KETO NPs in terms of maintaining colloidal stability over 30 minutes, with increase in size remaining ~ 200 %.

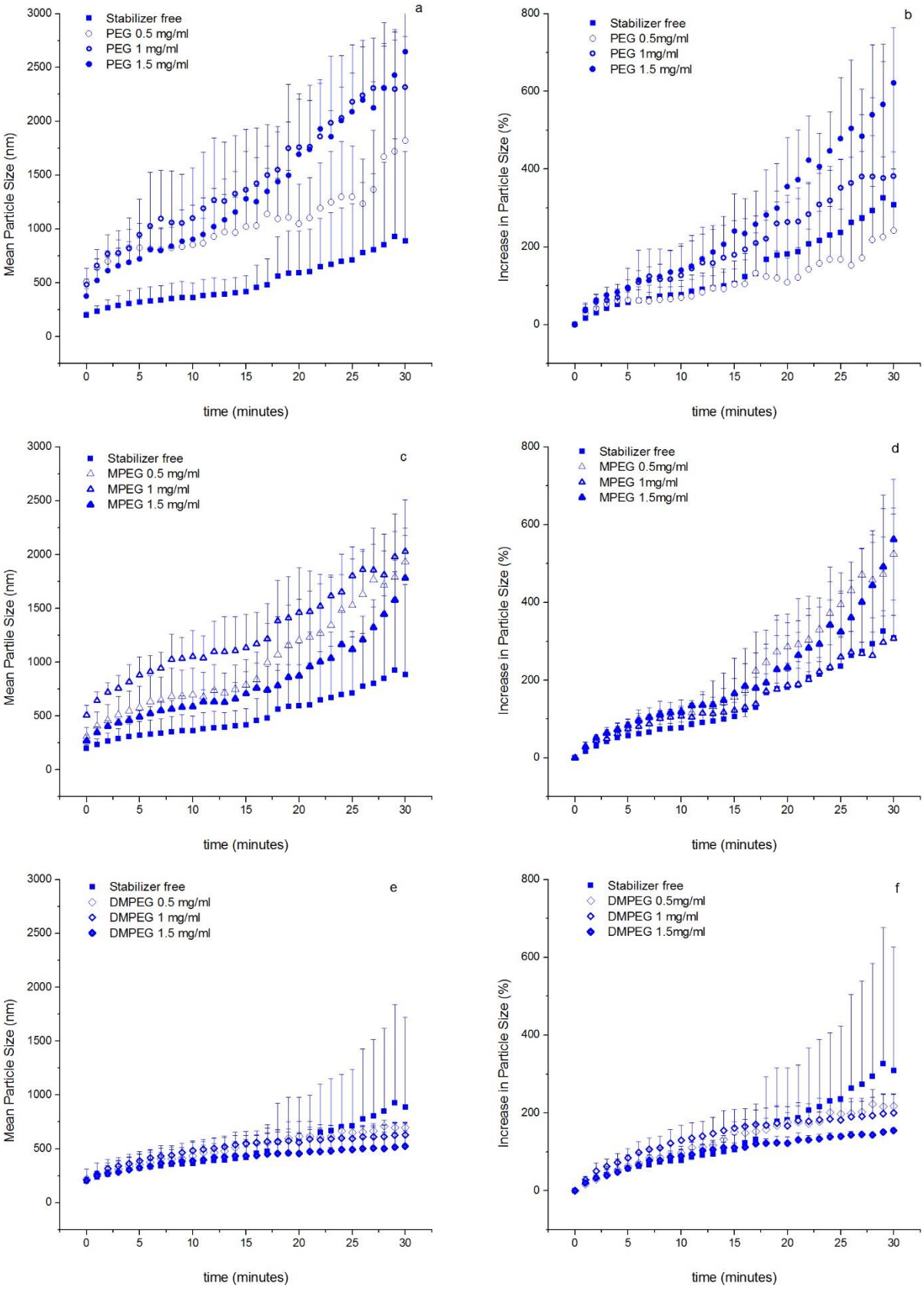

328

329 **Fig. 6.** Mean particle size (nm) and increase in particle size (%) versus time (minutes) for KETO NPs

330 stabilized with (a and b) PEG (c and d) MPEG and (e and f) DMPEG.

In summary, the most effective stabiliser for all the APIs investigated, although marginally for KETO, was DMPEG. In all cases, stabilization was polymer concentration dependent as seen in Fig. SI. 4. Wang et al., (2011) have previously shown this to be the case, suggesting polymer (acting as steric stabilizer) concentration affects efficacy of stabilization. More importantly that, an optimum concentration of stabilizer is required as an inadequate amount of stabilizer can result in incomplete coverage of API particle surfaces. It seems logical, in some instances that beyond the optimum stabilizer concentration, all API particle surface adsorption sites are occupied and a further increase in stabilizer concentration is of no benefit in terms of stabilization. We have observed that effective stabilizer concentration is dependent upon both API and stabilizer structure, similar to the findings of Wang et al., (2011). As the three structurally similar APIs (Fig. 1) studied in this work were all effectively stabilized by the same polymer, DMPEG, we can conclude that a structural component common to all three APIs is responsible for this stabilization. Choi et al. (2005) concluded that polymers with higher hydrophobicity successfully produced stable nanocrystals of hydrophobic drugs in comparison to those with lower hydrophobicity. This was attributed to the strong polymer adsorption onto the hydrophobic drug surfaces (Choi et al., 2005). DMPEG possesses greater hydrophobic character in comparison to PEG and MPEG. Hence, it is possible that improved surface coverage owing to DMPEG's stronger interaction with the API particle surfaces, resulted in greater stabilization of the resultant NPs.

Fig. SI. 5 reveals an initial increase in ITR derived count rate, followed by a decrease and eventual plateau in mean count rate (Hassan et al., 2015). This initial increase in mean count rate correlates with a precipitation burst in ITR NP growth, beyond this point sufficient ITR growth site coverage by the stabilizer inhibits NP aggregation and slower NP growth can be seen. Fig. SI. 6 and 7 also reveal a general trend of falling and eventual plateau in count rates for POS and KETO NPs. This provides suggestion that, Ostwald ripening, whereby particle solubility increases as the radius decreases via the Gibbs-Thomson effect, might be at play. Falling count rates may represent larger particles growing at the expense of their smaller counterparts.

3.2 Solid State Characterisation of NPs

All starting components (APIs and polymers) were crystalline in nature (Fig. 7 and SI. 8). ITR NPs stabilized by 0.5 mg/ml DMPEG appear amorphous from PXRD data shown in Fig. 7b however work carried out by Mugheirbi and Tajber (2015a) has proven ITR NPs form stable liquid crystal structures with a nematic phase. POS has been reported to exhibit rich solid state polymorphism (Andrews et al., 2004; Wieser et al., 2012 and 2013). Crystalline POS polymorph form III is denoted in Fig. 7c (Andrews et al., 2004). In this study, the POS polymorphic form used to formulate these NPs was the more stable POS polymorph crystalline form I, denoted in Fig. 7d (Andrews et al., 2004). Within approximately 5 minutes of formation, POS NPs can be isolated in an amorphous phase, as confirmed by the diffractogram shown in Fig. 7f, which crystallises to form I within 30 minutes (Fig. 7e). Crystallisation of amorphous POS was also seen in studies of Mugheirbi et al. (2017) on spheres coated with solid dispersions containing either ITR or POS, which led to a decrease in the release rate of POS. It was not possible to isolate KETO NPs immediately upon formation for PXRD studies, however these NPs were confirmed as PXRD crystalline at 30 minutes as seen in Fig. 7h. Crystalline nature of KETO NPs has been observed elsewhere in the literature (Lui et al., 2011).

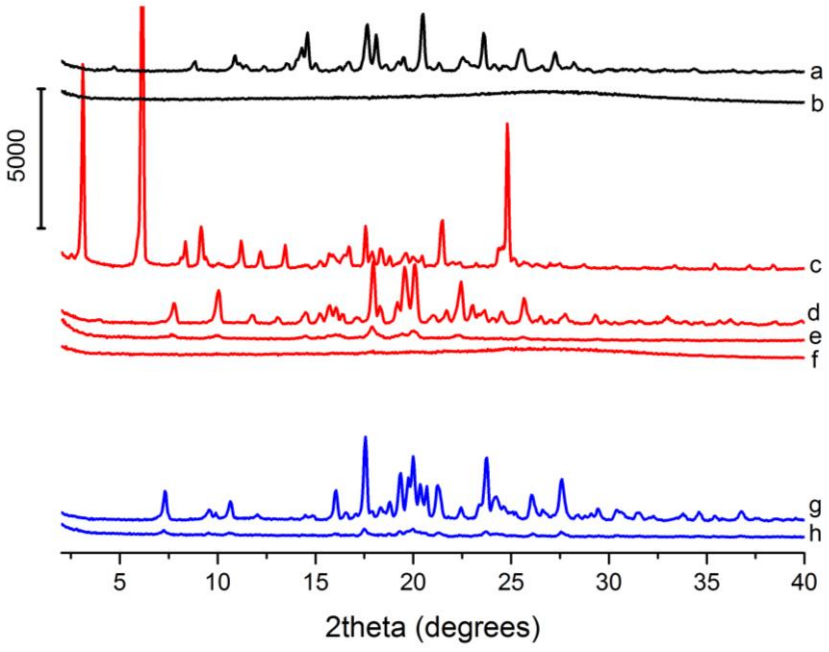

Fig. 7. PXRD diffraction patterns of (a) crystalline ITR (b) ITR NPs stabilised by 0.5 mg/ml DMPEG at 0 minutes (c) crystalline POS polymorph form III (d) crystalline POS polymorph form I (e) POS polymorph form I stabilizer free NPs at 30 minutes (f) amorphous POS stabilizer free NPs at 0 minutes (g) crystalline KETO (h) KETO – MPEG 0.5 mg/ml NPs at 30 minutes.

3.3 Particle morphology

SEM images displayed in Fig. 8 confirm that the NPs were in the nanometre-size range. Fig. 8a reveals ITR NPs with porous nature when DMPEG 1 mg/ml was used, at 30 minutes. Pin prick "blowholes" present on nanoparticle surfaces provide evidence of the hollow structure of the NPs (Fig. 8b and c). This supports the theory proposed by Mugheirbi et al., (2014) whereby particles are formed via solidification of droplets through counter diffusion of solvent and anti-solvent (Mugheirbi and Tajber, 2015a).

POS crystal structures can be seen in Fig. 8d, these are plate-like in structure with dendritic ends and particle size above 2 micron. The red circle in this image also shows amorphous POS NPs present alongside these crystalline structures. This, in conjunction with increase in particle size data (Fig. 5) and PXRD analysis (Fig. 7e and f), suggests that POS NPs underwent a solid state transformation over the 30 minutes. Saturation solubility differences between amorphous and crystalline POS NPs initiated a process similar to Ostwald ripening, leading to a rapid conversion of amorphous NPs into the crystalline state. Fig. 8c reveals peanut shaped POS NPs. This confirms that a number of stages exist during nanoparticle formation and growth including a "break-up" stage, with two daughter particles originating from an original mother particle.

Fig. 8e confirms the spherical nature of KETO NPs when no stabilizer is included in the system, as well as a particle size below 1 micron. Fig. 8f shows a rougher texture present on the KETO NP surface when PEG 0.5 mg/ml was included as a stabilizer in the system. The rough texture that can be observed on

396 the surface of the nanoparticles in Fig. 8a, g, h can be attributed to the stabilizer presence on API

397 particle surfaces.

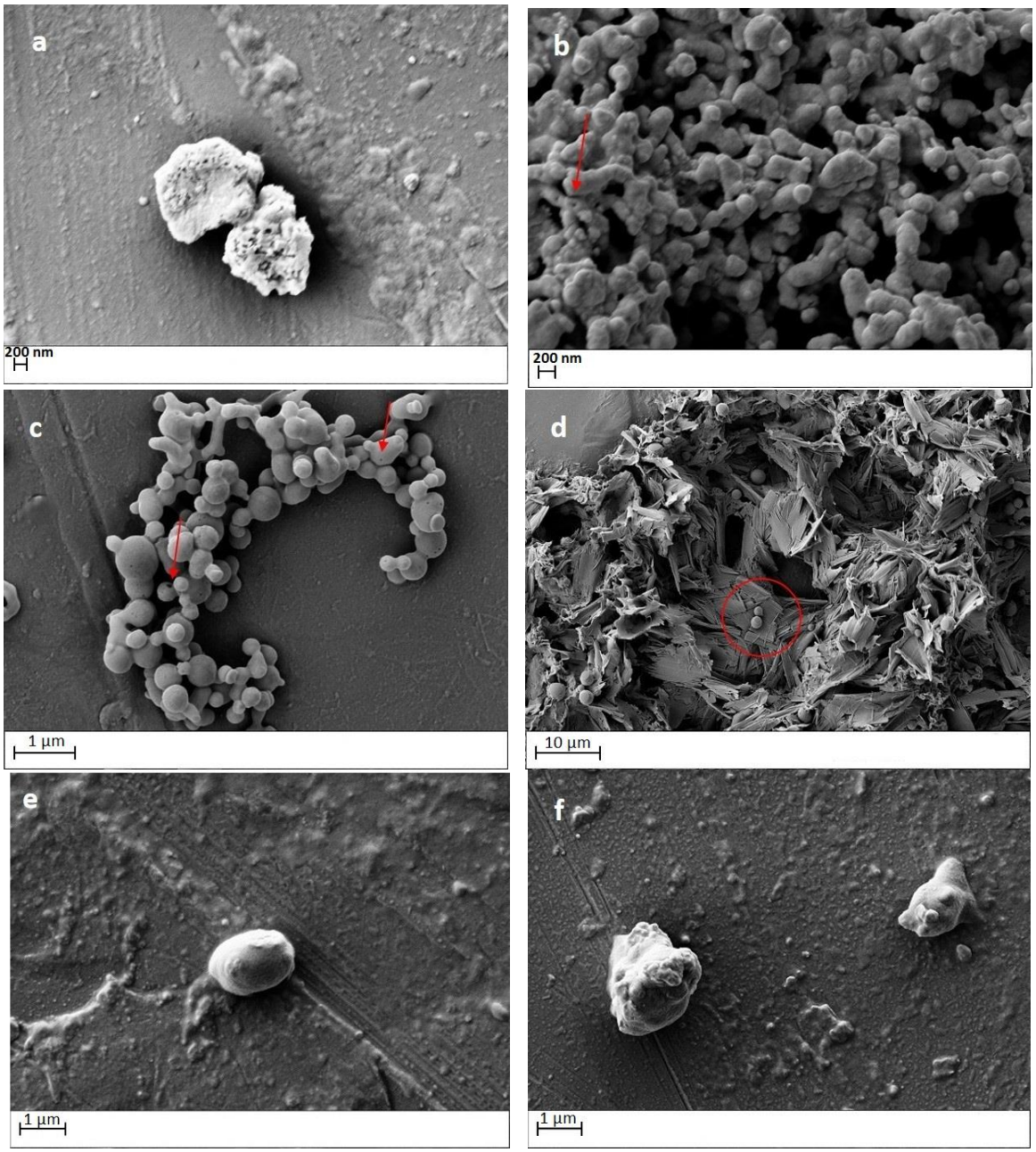

398

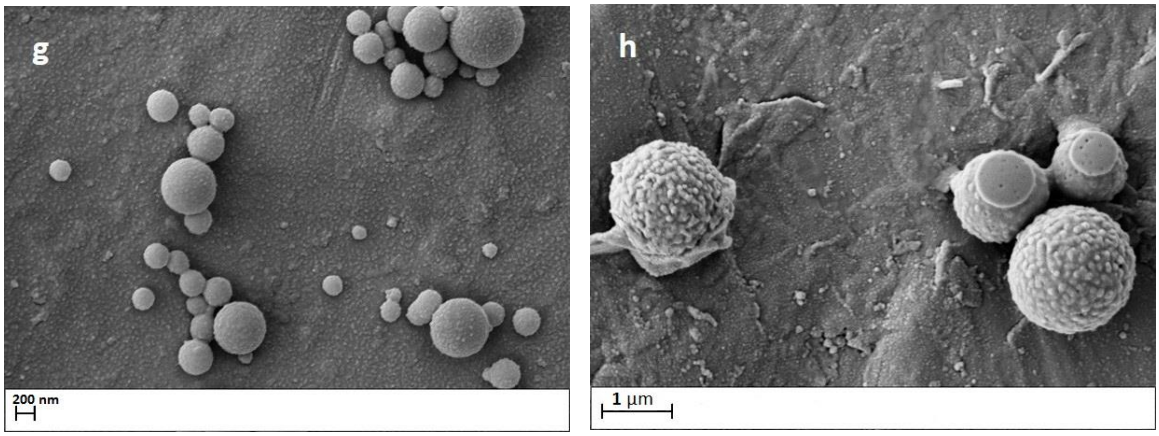

Fig. 8. Scanning electron micrograph of (a) ITR NPs with DMPEG 1 mg/ml at 30 minutes (b) ITR NPs with DMPEG 0.5 mg/ml at 30 minutes (c) POS NPs with MPEG 0.5 mg/ml at 0 minutes (d) POS NPs with DMPEG 0.5 mg/ml at 30 minutes (e) KETO NPs with no stabilizer at 30 minutes (f) KETO NPs with PEG 0.5 mg/ml at 0 minutes (g) POS NPs with PEG 1 mg/ml at 0 minutes and (h) POS NPs with DMPEG 0.5 mg/ml at 30 minutes. (Hollow particle indicated by red arrow).

3.4 Mechanism of Particle Growth/Size Increase

Attempts were made to fit mean particle size data using a kinetic growth model. The hybrid crystal growth model described in Eq. 1 was employed to gain knowledge surrounding the mechanisms involved in particle growth. Understanding the factors that affect the kinetics of crystal growth provides key information necessary for the fine-tuning of nanoparticle properties. Elsewhere in the literature the process of Ostwald ripening has been described using kinetic models (Wagner, 1961; Speight, 1968; Kirchner, 1971). Kinetic modelling of DLS data focused on DMPEG, as it proved to be the most effective stabilizer for all API nanodispersions. In addition, all other polymers encouraged crystallization of POS NPs, therefore fitting of this data was simply not possible. This hybrid crystal growth considers the particle size at any time is the result of two processes orientated attachment (OA) and Ostwald ripening (OR) occurring simultaneously:

$$\boldsymbol{D} = \frac{\boldsymbol{D_0}\left(\sqrt[3]{\boldsymbol{2k_1}}\boldsymbol{t}+\boldsymbol{1}\right)}{(\boldsymbol{k_1}\,\boldsymbol{t}+\boldsymbol{1})} + \boldsymbol{k_2}\,\boldsymbol{t}^{\boldsymbol{1/n}} \qquad \text{Eq. 1}$$

where D is the particle diameter at any time , D_0 is the initial particle diameter, k_1 is the rate constant for the OA process, k_2 is the rate constant for the OR process, t is time in hours and n is an exponent describing the relevant coarsening mechanism (Huang et al., 2003a; Yin et al., 2011).

When the exponent n = 2, nanoparticle growth is said to be interface controlled and when n = 3 growth is diffusion controlled (Wagner, 1961; Speight, 1968; Kirchner, 1971). Parabolic growth has been associated with interface controlled growth whereas cubic growth is characteristic of diffusion controlled coarsening (Wagner, 1961). Fig. SI 9 provides evidence of growth following a parabola trend for KETO NPs stabilized with DMPEG 1.5 mg/ml. This trend was present for all APIs stabilized with DMPEG at a concentration of 1.5 mg/ml. These growth curves should be best fitted as a full data set hybrid crystal growth kinetic model (see Tables 3 to 5). This would be characteristic of interface controlled growth kinetics. In contrast, Fig. SI 10 and 11 provides evidence of cubic growth kinetics. This trend was evident for all nanodispersions aside from those stabilized by DMPEG 1.5 mg/ml, for this reason such datasets were fitted in two separate stages (Huang et al., 2003b). This cubic growth tends to be associated with diffusion controlled particle coarsening.

Growth curves were either fitted as a single phase of growth indicated by asterisks (*) in Table 3 to 5 and Fig. SI 9, or as two separate stages of growth (Table 3 to 5 and Fig. SI 10 and 11). Fitting parameters are presented in Table 3 with results supporting growth via Eq.1 growth model. Initially, the data was fitted with the full model including OA and OR mechanisms, however it was not possible to achieve a good fit doing so. Thus it was concluded that the particle size growth of azole antifungal NPs described in this work cannot be explained by the OA process. For this reason, it was necessary to fix the k_1 constant to zero, therefore one can assume that particle coarsening is driven solely by the OR process. In addition, D_0 values were fixed according to particle size. Also, when fitted as two separate stages of growth, D_0 for part B was fixed as the particle size at the beginning of part B.

Table 3. Summary of parameters obtained by fitting Eq. 1 to experimental data of mean particle size of ITR NPs. The stabilizer used was DMPEG.

	Part A				Part B			
Sample	Time (h)	D_0 (nm)	$k_2 \pm SE$ ($nm^n \bullet h^{-1}$)	n ± SE	Time (h)	D_0 (nm)	$k_2 \pm SE$ ($nm^n \bullet h^{-1}$)	n ± SE
0 mg/ml	0 - 0.18	155	170 ± 11.5	2.5 ± 0.2	0.18-0.5	239	598 ± 68	0.4 ± 0.03
0.5 mg/ml	0 - 0.23	237	99 ± 6.5	3.4 ± 0.4	0.23-0.5	300	218 ± 78	0.4 ± 0.05
1 mg/ml	0 - 0.15	218	92 ± 6	3.7 ± 0.4	0.15-0.5	272	239 ± 32	0.5 ± 0.04
1.5 mg/ml	0 - 0.15	131	451 ± 123	4.3 ± 2.0	0.15-0.5	300	412 ± 47	0.8 ± 0.07
1.5 mg/ml*	0 – 0.5	131	787 ± 46	1.5 ± 0.04	N/A	N/A	N/A	N/A

* - full dataset was fitted

Table 4. Summary of parameters obtained by fitting Eq. 1 experimental data of mean particle size of POS NPs. The stabilizer used was DMPEG.

	Part A				Part B			
Sample	Time (h)	D_0 (nm)	$k_2 \pm SE$ ($nm^n \bullet h^{-1}$)	n ± SE	Time (h)	D_0 (nm)	$k_2 \pm SE$ ($nm^n \bullet h^{-1}$)	n ± SE
0 mg/ml	0 - 0.27	280	795 ± 36	1.69 ± 0.07	0.27 - 0.5	627	2744 ± 718	0.29 ± 0.03
0.5 mg/ml	0 - 0.42	245	911 ± 45	2.12 ± 0.15	0.42 - 0.5	813	$3.3 \bullet 10^6 \pm 4.3 \bullet 10^6$	0.07 ± 0.01
1 mg/ml	0 - 0.23	242	1644 ± 78	1.35 ± 0.05	0.23 - 0.5	785	$1.3 \bullet 10^9 \pm 4.2 \bullet 10^6$	0.04 ± 0.01
1.5 mg/ml	0 - 0.23	238	517 ± 220	980 ± 170128	0.23 - 0.5	785	2136 ± 1815	0.28 ± 0.08
1.5 mg/ml*	0 - 0.5	238	1103 ± 28	1.69 ± 0.06	N/A	N/A	N/A	N/A

* - full dataset was fitted

Table 5. Summary of parameters obtained by fitting Eq. 1 experimental data of mean particle size of KETO NPs. The stabilizer used was DMPEG.

	Part A				Part B			
Sample	Time (h)	D_0 (nm)	$k_2 \pm SE$ ($nm^n \bullet h^{-1}$)	n ± SE	Time (h)	D_0 (nm)	$k_2 \pm SE$ ($nm^n \bullet h^{-1}$)	n ± SE
0 mg/ml	0 - 0.25	190	469 ± 16	1.9 ± 0.06	0.25 – 0.5	418	3959 ± 694	0.3 ± 0.02
0 mg/ml*	0 - 0.5	190	462 ± 97	351 ± 14425	N/A	N/A	N/A	N/A
0.5 mg/ml*	0 - 0.5	220	815 ± 17	1.4 ± 0.03	N/A	N/A	N/A	N/A
1 mg/ml*	0 - 0.5	210	600 ± 13	2.2 ± 0.08	N/A	N/A	N/A	N/A
1.5 mg/ml*	0 - 0.5	200	466 ± 7	2.0 ± 0.05	N/A	N/A	N/A	N/A

* - full dataset was fitted

Fitting of the model presented in Eq. 1 to ITR NP datasets suggests that OR growth is controlled by bulk diffusion in the first stage of growth where n ~ 3 and above (Table 3). Interestingly, the second stage of growth is characterised by n < 1, this would suggest a change to interface controlled growth (Table 3). Logically, the adsorption of stabilizers onto ITR particle surfaces may be a time dependent process and therefore their role may be one of greater importance in the later stages of OR. The ITR k_2 OR rate constant is lower in the first stage of growth compared with the second stage, aside from DMPEG 1.5 mg/ml. This suggests the rate of OR increases as time proceeds.

According to Table 4, in the first stage of growth for POS NPs the k_2 OR rate constant increases with increasing stabilizer concentration. In this instance DMPEG may achieve the opposite of stabilization, encouraging OR for POS NPs as well as providing a driving force for the crystallisation process. This may also explain the large and meaningless *n* exponent obtained for POS DMPEG 1.5 mg/ml during the first stage of growth. During the second phase of growth, k_2 OR rate constant values become extremely large and meaningless, this may be caused by the rapid crystallisation taking place as confirmed by PXRD and SEM.

Stabilizer free KETO NPs exhibited cubic growth associated with bulk diffusion controlled growth, causing the *n* exponent to be meaningless when this data was fitted a single (FULL) phase (Table 5). Introducing a stabilizer forces the OR process to transition to an interface controlled growth (n ~ 2) associated with parabolic growth seen in Fig. SI. 9. KETO NPs stabilised by polymers were therefore fitted as a single stage as denoted by an asterisk in Table 5. Increasing DMPEG concentration causes the KETO k_2 OR rate constant to decrease, suggesting the stabilizer in this instance is effectively hindering the OR process in a concentration dependent manner (Fig. 6f).

Furthermore, all NPs stabilized by DMPEG 1.5 mg/ml exhibit parabolic growth, characteristic of interface controlled growth, confirmed by n exponent values ~ 2. It should be noted, that ITR k_2 OR rate constant values are the lowest of all APIs, suggesting OR is slowest for these NPs (Table 3) thereby granting them greatest colloidal stability.

The role of surface adsorption in growth kinetics remains a complicated one. It is possible that the stabilizers employed in this study have multiple, conflicting roles. It seems likely that the presence of stabilizers has a steric hindrance effect achieved via long flexible polymer carbon chains. These chains provide an energy barrier to the bulk diffusion process forcing OR to become interface controlled. In the case of ITR, addition of a stabilizer appears to decrease the rate of the OR growth (Table 3). However, stabilizer concentration appears to be of great importance, with a concentration threshold existing whereby below this, inhibition of OR exists and above it, OR is promoted. For KETO NPs, increasing stabilizer concentration appears to exclusively inhibit OR growth confirmed by the decreasing k_2 OR rate constants in Table 5. Stabilizers appear to promote OR growth in the case of POS NPs, shown by k_2 OR rate constants in Table 3.

3.5 Solid State Transformation of NP in Dispersions over Time

The three APIs made into NPs and investigated in this work undergo different crystallization pathways. Particles existing in solution that interact through Brownian motion are capable of aggregating to form larger structures via numerous pathways.

ITR NPs possess liquid crystalline structures, with a nematic phase upon initial formation as shown previously (Mugheirbi and Tajber, 2015a). Molecules that induce liquid crystallinity are referred to as mesogens, they tend to be needle like or disk like in structure, making ITR an ideal candidate. As Mugheirbi and Tajber (2015a) have shown, the absence of H-bond donor groups within the ITR structure means that Π- Π stacking is likely to be responsible for stabilizing ITRs liquid crystalline structure (Fig. 1). The ability to form these liquid crystalline phases may contribute to very good ITR NP colloidal stability and delayed crystallisation seen beyond 30 minutes. However, the liquid

497 crystalline phase of ITR has a higher solubility than the crystalline phase and, as observed by Mugheirbi
498 and Tajber (2015b), can lead to crystallisation of the drug, via the OR mechanism to microcrystals. NP
499 production via wet media milling has been shown to preserve the crystalline nature of ITR NPs (Liu et
500 al., 2011). The method of production has a profound impact upon the crystallisation pathways taken
501 by ITR.

502 POS particles associate in an unstructured way and are therefore amorphous in nature, with a
503 tendency to crystallize quickly within 30 minutes as confirmed by Fig. 7e and 8d. Amorphous-to-
504 crystalline pathways have a thermodynamic origin, with aggregation of metastable amorphous
505 particles followed by transformation to a final thermodynamically stable ordered crystalline
506 polymorph form I (Wieser et al., 2012). This strong tendency to crystallize can be attributed to the
507 presence of a hydroxyl group within the chemical structure of POS, therefore responsible for hydrogen
508 bonding within its crystal lattice (Fig. 1). Strong hydrogen bonding between colliding NPs increases the
509 likelihood that they will coalesce together.

510 Unfortunately, it was not possible to isolate KETO NPs upon initial formation however, it is possible
511 that amorphous particles were generated at this stage. PXRD data shown in Fig. 7h confirm the
512 crystalline nature of KETO NPs at 30 minutes, however the peak intensities are below those of the
513 starting material powder. The amorphous character of KETO NPs produced via high pressure
514 homogenisation has been noted elsewhere in the literature (Kakkara et al., 2015). Also, KETO has
515 shown itself to be resistant to solid state changes, maintaining its crystallinity when milled for NP
516 production (Liu et al., 2011). This reiterates the profound impact NP production method has upon
517 crystallisation pathways.

518 ITR, POS and KETO NPs produced in this work crystallised over time, however a less ordered precursor,
519 preceding the full crystallisation, was isolated or likely to be formed in each case. It therefore appears
520 that these APIs proceed via “non-classical crystallization” routes involving kinetically metastable
521 amorphous/disordered precursor particles (Niederberger and Cölfen, 2006). This presents limitations

in terms of the application of Eq. 1. as it is therefore possible that alternative physical processes are competing alongside OR growth. Nevertheless, fitting parameters confirm that ITR NPs experience the slowest rate of OR. The rate of OR appears to be inherent of the crystallisation pathway by which these APIs proceed.

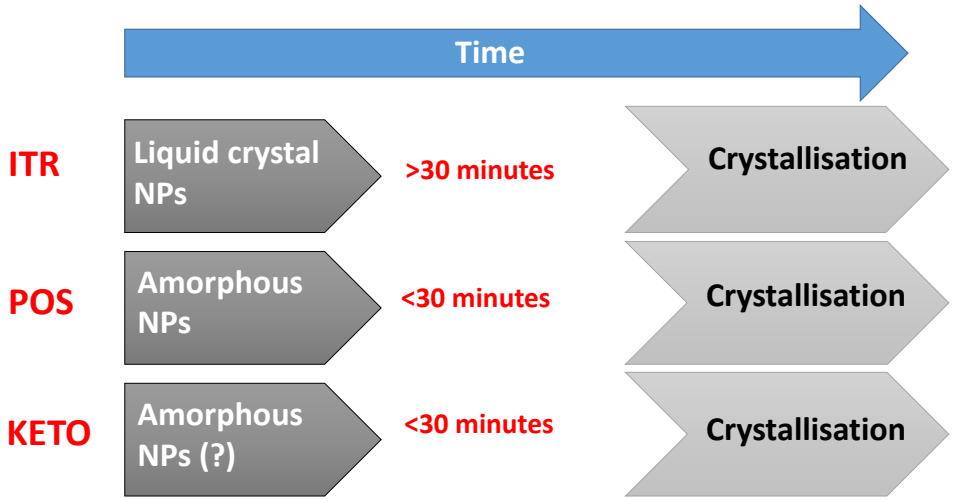

Fig. 9. Schematic representation of API crystallisation pathways. ITR = itraconazole, POS = posaconazole, KETO = ketoconazole, NPs = nanoparticles.

4. Conclusions

Nano-dispersions made of ITR, POS and KETO were formed by anti-solvent precipitation and characterised using a number of physical techniques. ITR NPs have the greatest colloidal stability when no stabilizer is included in the system, when compared with POS and KETO NP equivalents. It appears that the stabilizers employed in this study may have multiple, conflicting roles. DMPEG proved to be the most effective stabilizer for all APIs in these conditions. The greater hydrophobic content of DMPEG, in comparison to MPEG and PEG, appears to affect strength of stabilizer adsorption onto API particle surfaces and hence stabilization of NPs. In general, the presence of DMPEG causes OR growth to become an interface controlled process. Interestingly, DMPEG encourages OR for POS NPs and drives the crystallisation process. It cannot therefore be assumed the role of stabilizers to be confined to stabilization alone. The rate of OR appears to be inherent of the crystallisation pathway by which

these APIs proceed. Crystallization mechanisms are API, stabilizer and stabilizer concentration dependent. These three structurally similar APIs undergo different crystallization pathways. It appears that stabilization of NP system is dependent upon three factors: API chemical structure, crystallisation pathway and theoretical supersaturation ratio. Further work will look to improve our understanding behind the mechanism of stabilization for these NP systems and the role of stabilizers within these crystallization pathways.

5. Acknowledgements

Research leading to these results was supported by the Synthesis and Solid State Pharmaceutical Centre (SSPC), financed by a research grant from Science Foundation Ireland (SFI) and co-funded under the European Regional Development Fund (Grant Number 12/RC/2275). The authors would like to thank Dr. Grzegorz Garbacz (Physiolution GmbH, Germany) for kindly supplying itraconazole.

6. References

Andrews, D.R., Leong, W., Sudhakar, A., 2004. United States Patent US006958337B2.

Butler, J.M., Dressman, J.B., 2010. The Developability Classification System: Application of Biopharmaceutics Concepts to Formulation Development. J. Pharm. Sci. 99, 4940–4954.

Choi, J., Youn, J., Kwak, H., Uk, B., Lee, J., 2005. Role of polymeric stabilizers for drug nanocrystal dispersions. Curr. Appl. Phys. 5, 472–474.

Dolenc, A., Kristl, J., 2009. Advantages of celecoxib nanosuspension formulation and transformation into tablets. Pharm. Nanotechnol. 376, 204–212.

Dressman, J.B., Reppas, C., 2000. In vitro-in vivo correlations for lipophilic, poorly water-soluble drugs. Eur. J. Pharm. Sci. 11, 73–80.

Ghosh, I., Schenck, D., Bose, S., Ruegger, C., 2012. European Journal of Pharmaceutical Sciences Optimization of formulation and process parameters for the production of nanosuspension by

564 wet media milling technique: Effect of Vitamin E TPGS and nanocrystal particle size on oral
565 absorption. Eur. J. Pharm. Sci. 47, 718–728.

566 Han, T.Y.J., Aizenberg, J., 2007. Calcium Carbonate Storage in Amorphous Form and Its Template-
567 Induced Crystallization. Chem. Mater. 20, 1064–1068.

568 Hassan, P., Rana, S., Verma, G., 2015. Making sense of brownian motion: colloid characterization by
569 dynamic light scattering. Langmuir. 31, 3–12.

570 Huang, F., Zhang, H., Banfield, J.F., 2003a. The Role of Oriented Attachment Crystal Growth in
571 Hydrothermal Coarsening of Nanocrystalline ZnS. J. Phys. Chem. B. 107, 10470–10475.

572 Huang, F., Zhang, H., Banfield, J.F., 2003b. Two-stage crystal-growth kinetics observed during
573 hydrothermal coarsening of nanocrystalline ZnS. Nano Lett. 3, 373–378.

574 Ilevbare, G., Taylor, L.S., 2013. Liquid-Liquid Phase Separation in Highly Supersaturated Aqueous
575 Solutions of Poorly-Water Soluble Drugs – Implications for Solubility Enhancing Formulations.
576 Cryst. Growth Des. 13, 1497–1509.

577 Ingham, B., Lim, T.H., Dotzler, C.J., Henning, A., Toney, M.F., Tilley, R.D., 2011. How Nanoparticles
578 Coalesce : An in Situ Study of Au Nanoparticle Aggregation and Grain Growth. Chem. Mater. 23,
579 3312–3317.

580 Kakkara, S., Karuppayilb, S.M., Rauta, J.S., Giansantic, F., Papuccid, L., Schiavonee, N., Kaura, I.P.,
581 2015. Lipid-polyethylene glycol based nano-ocular formulation of ketoconazole. Int. J. Pharm.
582 495, 276-289.

583 Kirchner, H.O., 1971. Coarsening of grain-boundary precipitates. Metall. Trans. 2, 2861–2864.

584 Liu, P., Rong, X., Laru, J., Van Veen, B., Kiesvaara, J., Hirvonen, J., Laaksonen, T., Peltonen, L., 2011.
585 Nanosuspensions of poorly soluble drugs: Preparation and development by wet milling. Int. J.
586 Pharm. 411, 215–222.

587 Mahesh, K.V., Singh, S.K., Gulati, M., 2014. A comparative study of top-down and bottom-up
588 approaches for the preparation of nanosuspensions of glipizide. Powder Technol. 256, 436–
589 449.

590 Matteucci, M.E., Paguio, J.C., Miller, M.A., Williams, R.O., Johnston, K.P., 2009. Highly supersaturated
591 solutions from dissolution of amorphous Itraconazole microparticles at pH 6.8. Mol. Pharm. 6,
592 375–385.

593 Mugheirbi, N.A., Paluch, K.J., Tajber, L., 2014. Heat induced evaporative antisolvent
594 nanoprecipitation (HIEAN) of itraconazole. Int. J. Pharm. 471, 400–411.

595 Mugheirbi, N.A., Tajber, L., 2015a. Mesophase and size manipulation of itraconazole liquid
596 crystalline nanoparticles produced via quasi nanoemulsion precipitation. Eur. J. Pharm.
597 Biopharm. 96, 226–236.

598 Mugheirbi, N.A., Tajber, L., 2015b. Crystal habits of itraconazole microcrystals: unusual isomorphic
599 intergrowths induced via tuning recrystallization conditions. Mol. Pharmaceutics. 12, 3468–
600 3478.

601 Mugheirbi, N.A., O'Connell, P., Serrano, D.R., Healy, A.M., Taylor, L.S., Tajber L., 2017. A comparative
602 study on the performance of inert and functionalized spheres coated with solid dispersions
603 made of two structurally related antifungal drugs. Mol. Pharmaceutics, 14, 3718–3728.

604 Niederberger, M., Cölfen, H., 2006. Oriented attachment and mesocrystals: non-classical
605 crystallization mechanisms based on nanoparticle assembly. Phys. Chem. Chem. Phys. 8, 3271–
606 3287.

607 Noyes, A.A., Whitney, R., 1897. The rate of solution of solid substances in their own soltuions. J. Am.
608 Chem. Soc. 19, 930–934.

609 Ostwald, W., 1900. Über die vermeintliche Isomerie des roten und gelben Quesck-silberoxyds und
610 die Oberflachenspannung fester Körper. Z. Phys. Chem. 34, 495–503.

611 Palla, B.J., Shah, D.O., 2002. Stabilization of High Ionic Strength Slurries Using Surfactant Mixtures:
612 Molecular Factors That Determine Optimal Stability. J. Colloid Interface Sci. 256, 143–152.

613 Rane, S.S., Choi, P., 2005. Polydispersity index: How accurately does it measure the breadth of the
614 molecular weight distribution? Chem. Mater. 17, 926.

615 Shang, J., Gao, X., 2014. Nanoparticle counting: towards accurate determination of the molar
616 concentration. Chem. Soc. Rev. 43, 7267–7278.

617 Shegokar, R., Müller, R.H., 2010. Nanocrystals: Industrially feasible multifunctional formulation
618 technology for poorly soluble actives. Int. J. Pharm. 399, 129–139.

619 Speight, M.V., 1968. Growth kinetics of grain-boundary precipitates. Acta. Metall. 16, 133–135.

620 Van Eerdenbrugh, B., Van de Mooter, G., Augustijins, P., 2008. Top-down production of drug
621 nanocrystals: Nanosuspension stabilization, miniaturization and transformation into solid
622 products. Int. J. Pharm. 364, 64-75.

623 Van Eerdenbrugh, B., Vermant, J., Martens, J.A., Froyen, L., Van Humbeeck, J., Augustijns, P., Van
624 Den Mooter, G., 2009. A screening study of surface stabilization during the production of drug
625 nanocrystals. J. Pharm. Sci. 98, 2091-2103.

626 Viswanatha, R., Sarma, D.D., 2007. Growth of Nanocrystals in Solution. Nanomaterials Chemistry:
627 Recent Developments and New Directions. 139-170.

628 Voorhees, P.W., 1985. The Theory of Ostwald ripening. J. Sat. Phys. 38, 231–252.

629 Wagner, C.Z., 1961. Theory of precipitate change by redissolution. Elektrochem. 65, 581–591.

630 Wang, H., Pan, Q., Rempel, G.L., 2011. Micellar nucleation differential microemulsion
631 polymerization. Eur. Polym. J. 47, 973–980.

632 Wieser, J., Pichler, A., Hotter, A., Griesser, U., Langes, C., 2013. Patent Number US 8,563,555 B2.

633 Wieser, J., Pichler, A., Hotter, A., Griesser, U., Langes, C., 2012. Patent Number US 2012/0101277 A1.

634 Yin, S., Huang, F., Zhang, J., Zheng, J., Lin, Z., 2011. The Effects of Particle Concentration and Surface
635 Charge on the Oriented Attachment Growth Kinetics of CdTe Nanocrystals in H2O. J. Phys.
636 Chem. C. 115, 10357–10364.

637 Zhang, Z., Shen, Z., Wang, J., Zhao, H., Chen, J., Yun, J., 2009. Nanonization of megestrol acetate by
638 liquid precipitation. Ind. Eng. Chem. Res. 48, 8493–8499.